Specific ^{18}F-FDHT Accumulation in Human Prostate Cancer Xenograft Murine Models Is Facilitated by Prebinding to Sex Hormone–Binding Globulin

Benjamin M. Larimer[1], Frank Dubois[1], Emily Bloch[1], Sarah Nesti[1], Michael Placzek[1], Giorgia Zadra[2,3], Jacob M. Hooker[1], Massimo Loda[2,3], and Umar Mahmood[1]

[1]Athinoula A. Martinos Center for Biomedical Imaging, Department of Radiology, Massachusetts General Hospital, Boston, Massachusetts; [2]Department of Medical Oncology, Center for Molecular Oncologic Pathology, Dana-Farber Cancer Institute, Harvard Medical School, Boston, Massachusetts; and [3]Department of Pathology, Brigham and Women's Hospital, Harvard Medical School, Boston, Massachusetts

Tremendous efforts are currently dedicated to the development of novel therapies targeting the androgen receptor (AR), the major driver of prostate cancer disease and its progression to castration resistance. The ability to noninvasively interrogate AR expression over time in murine models of prostate cancer would permit longitudinal preclinical analysis of novel compounds that could not otherwise be accomplished ex vivo. Although PET imaging with 16β-^{18}F-fluoro-5α-dihydrotestosterone (^{18}F-FDHT) has successfully quantified AR levels clinically, no rodent model of ^{18}F-FDHT imaging has been reported so far. One difference between humans and rodents is the absence in the latter of the sex hormone–binding globulin (SHBG), a glycoprotein that binds to testosterone in the bloodstream, Here, we explore the role of SHBG in developing a working model of rodent AR imaging. **Methods:** Three human prostate cancer cell lines and xenografts (LNCaP, 22Rv1, and PC3) were used to examine the uptake of free ^{18}F-FDHT and SHBG-bound ^{18}F-FDHT. Both ligands were examined for stability and competitive binding to AR over time in vitro before in vivo studies. PET/CT imaging was used to dynamically measure the uptake of both tracers over 4 h, whereas specificity was determined by competitive binding with the AR antagonist enzalutamide. **Results:** AR levels correlated with the uptake of both ^{18}F-FDHT and SHBG-^{18}F-FDHT in prostate cancer cell lines. Interestingly, whereas both free and SHBG-bound ^{18}F-FDHT had a similar cellular accumulation at 1 and 2.5 h, SHBG-^{18}F-FDHT accumulated at significantly higher levels after 4 h—evidence that receptor-mediated uptake of SHBG accounted for later time-point differences. This observation was also seen in 22Rv1 tumor–bearing mice, in which SHBG-^{18}F-FDHT exhibited a significantly increased uptake (average tumor-to-background ratio [TBR], 1.62 ± 0.62) in comparison to unbound ^{18}F-FDHT (TBR, 0.81 ± 0.08) at 4 h. Furthermore, the specificity of the SHBG-^{18}F-FDHT accumulation at 4 h was demonstrated by a reduced tumor uptake after AR blockade with enzalutamide (TBR, 1.07 ± 0.13). **Conclusion:** Prebinding of ^{18}F-FDHT to SHBG allows accurate and quantitative PET imaging of AR levels in murine models of prostate cancer. This procedure may permit the use of PET imaging to study the longitudinal effects of AR-targeting therapies, accelerating novel-drug development.

Received Jan. 24, 2018; revision accepted May 3, 2018.
For correspondence or reprints contact: Umar Mahmood, Nuclear Medicine/Radiology, White 427, Massachusetts General Hospital, 55 Fruit St., Boston, MA 02114.
E-mail: umahmood@mgh.harvard.edu
Published online May 31, 2018.

Key Words: FDHT; SHBG; androgen receptor; prostate cancer

J Nucl Med 2018; 59:1538–1543
DOI: 10.2967/jnumed.118.208785

Prostate cancer is the second most common cause of cancer-related death and the cancer with the highest incidence in men. As such, prostate cancer is the focus of many novel therapeutics, including those that target the androgen receptor (AR) (*1*). Initially, most prostate cancers show a response to treatment by androgen deprivation because androgens are the physiologic growth factor for prostate cells (*2*). However, over time, almost all prostate cancers become unresponsive to treatment (*3*). These castration-resistant prostate cancers are difficult to manage and often lethal. The malignancy can develop through several mechanisms, but ultimately all lead to increased intracellular AR signaling (*4,5*). Despite the clinical relevance of AR quantification, histopathologic examinations of biopsy samples may be unable to provide an accurate characterization. In fact, clinical examination has demonstrated that AR expression levels can differ widely between metastatic sites in a single patient (*6*). Thus, the limited sampling of a biopsy is unable to capture the heterogeneity of AR expression across primary and metastatic sites of prostate cancer, making accurate quantification of AR levels difficult to obtain (*7*).

To overcome the limitations of biopsy, noninvasive imaging of AR can be used to quantify expression in both primary tumors and metastatic sites simultaneously, allowing for subsequent evaluation and guidance of AR-targeted therapies. PET offers a quantitative imaging technique that has been used extensively for both cancer detection and characterization in humans. Furthermore, an effective PET tracer for AR, 16β-^{18}F-fluoro-5α-dihydrotestosterone (^{18}F-FDHT), has already been used clinically to permit detection and relative quantification of AR expression noninvasively (*8*). ^{18}F-FDHT has been demonstrated to identify AR-positive lesions with high sensitivity and specificity in patients and to detect changes in AR over the course of therapy, suggesting that ^{18}F-FDHT is a promising candidate for use in monitoring AR clinically (*9*).

Although ^{18}F-FDHT PET imaging has been successful clinically, paradoxically, a mechanistic understanding in rodent tumor models has been lacking. This lack could be attributed to the

absence of sex hormone–binding globulin (SHBG) expression in most mature rodents, including mice, and previous ^{18}F-FDHT rodent studies support this hypothesis (*10*). A direct comparison of biodistribution was performed between immature rodents, which express a molecule similar to SHBG termed androgen-binding protein, and mature rats, which lack any FDHT-binding proteins (*10*). It was found that mature rodents had significant levels of accumulation in bone, presumably through defluorination of ^{18}F-FDHT, whereas immature rats did not, indicating a protective role of androgen-binding protein for ^{18}F-FDHT metabolism. Additionally, other species (e.g., nonhuman primates and rabbits) successfully imaged with ^{18}F-FDHT have serum SHBG or androgen-binding protein, but mice express no SHBG or analogs (*11,12*). The lack of positive results for ^{18}F-FDHT imaging in various rodents thus far led us to investigate whether ^{18}F-FDHT imaging can be improved in the mouse models of human prostate cancer most commonly used to assess novel androgen-modulating therapies. We brought about this improvement by binding ^{18}F-FDHT to SHBG and systematically studying the properties of the combination. A method to quantitatively monitor AR expression noninvasively in preclinical models of prostate cancer would permit repeated, global quantification of the receptor. This, in turn, could allow monitoring of the kinetics and outcomes of AR-modulating therapeutics.

In this study, we sought to accurately determine the effects of SHBG on ^{18}F-FDHT kinetics and biodistribution in mouse models of human prostate cancer. Specifically, we investigated whether it is possible to accurately quantify relative AR expression levels in mouse models of prostate cancer using ^{18}F-FDHT–based PET imaging and whether specific tumor uptake in these models can be improved using SHBG-bound ^{18}F-FDHT.

MATERIALS AND METHODS

Materials and Cell Lines

Unless otherwise stated, all chemicals were purchased from Sigma-Aldrich. LNCaP (CRL-1740), PC3 (CRL-1435), and 22Rv1 (CRL-2505) human prostate cells were purchased from ATCC and cultured in RPMI-1640 medium (ThermoFisher) supplemented with 10% fetal bovine serum (Aleken).

Murine Models

The mice were housed and maintained by the Center for Comparative Medicine following animal protocols approved by the Massachusetts General Hospital Institutional Animal Care and Use Committee. Male *nu/nu* mice were purchased from Charles River Laboratories. For tumor inoculation, approximately 1×10^6 cells were mixed in a 1:1 (v:v) ratio with Matrigel (Corning) and subcutaneously injected into the upper right flank of *nu/nu* mice. 22Rv1 xenograft models were injected in orchiectomized mice to simulate clinical castration conditions, whereas LNCaP xenografts, which require androgens for growth, were generated in intact mice.

^{18}F-FDHT Synthesis, Purification, and SHBG Interaction

^{18}F-FDHT was synthesized by modifying a procedure previously described in the literature (*13*). Crude ^{18}F-FDHT was purified by reversed-phase high-pressure liquid chromatography using a 9.4 × 250 mm Eclipse XDB-C18 (5 μm) column (Agilent) and eluted with 40% acetonitrile/60% 50 mM KH_2PO_4 at 4 mL/min. Nonradioactive peaks were analyzed by ultraviolet light (210 nm). Collected ^{18}F-FDHT was diluted with 20 mL of water and captured on a C18 light Sep-Pak cartridge (Waters) preconditioned with 1 mL of ethanol and 4 mL of water. ^{18}F-FDHT bound to the cartridge was washed with 5 mL of water and then eluted with ethanol and diluted with sterile 0.9% saline solution for a less than 10% final concentration of ethanol. Product purity and identity (coinjected with ^{18}F-FDHT) were confirmed by analytic high-pressure liquid chromatography using an Agilent Eclipse Plus-C18 (5 μm) eluting with 40% acetonitrile/60% 50 mM KH_2PO_4 at 2 mL/min (ultraviolet, 215 nm), with a retention time of 6.1 min. For experiments involving SHBG (Abcam)-bound ^{18}F-FDHT, 9 μg of purified recombinant human SHBG per mouse (54–108 mg of total protein) were incubated at 37°C for 30 min with approximately 740 MBq of ^{18}F-FDHT. Size-exclusion chromatography using a 10-kDa cartridge (GE Healthcare) was performed to eliminate free ^{18}F-FDHT. The final SHBG-^{18}F-FDHT complex was quantified by dose calibrator.

In Vitro Characterization of Free and SHBG-Bound ^{18}F-FDHT

Uptake of free ^{18}F-FDHT in LNCaP, 22Rv1, and PC3 prostate cancer cells was probed by incubating the purified radiotracer in 100 μL of serum-free medium with cells grown to 70% confluency in a 96-well tissue culture plate (Corning). Additional specificity for the AR was also determined by incubating separate wells of LNCaP cells with 10-fold dilutions of the AR antagonist enzalutamide (range, 0.1–100 μM) (Selekchem). After incubation with the probe, the cells were washed 3 times with 100 μL of Dulbecco phosphate-buffered saline (ThermoFisher) and lysed in 100 μL of 1% sodium dodecyl sulfate. Recovered cell lysate was assayed for radioactivity by a 2480 Wizard^2 automatic γ-counter (Perkin Elmer), and total protein was determined using the Pierce BCA Protein Assay Kit (Life Technologies) for standardization to total protein per well.

Competitive binding of enzalutamide to SHBG in the presence of ^{18}F-FDHT was assessed by the addition of 0.1–100 μM enzalutamide to SHBG before the addition of 0.37 MBq of ^{18}F-FDHT. The stability of both ^{18}F-FDHT and SHBG-^{18}F-FDHT was assessed by incubating the radiotracers with 100 μL of either phosphate-buffered saline, fetal bovine serum, or human serum for 1 h followed by cell-binding analysis as described previously. The specificity of SHBG-^{18}F-FDHT in comparison to ^{18}F-FDHT was analyzed by incubation of LNCaP cells grown to 70% confluency for 1 h with 0.37 MBq of the designated radiotracer in 100 μL of serum-free medium in the presence or absence of 100 μM enzalutamide, followed by quantification of cell lysate radioactivity and total protein. Finally, an examination of the temporal kinetics of cell binding of 0.37 MBq of either ^{18}F-FDHT or SHBG-^{18}F-FDHT was performed at 1, 2, and 4.5 h of incubation in LNCaP cells before lysis and quantification of total protein and radioactivity, in the same manner as described previously.

PET Imaging

Comparison of ^{18}F-FDHT and SHBG-^{18}F-FDHT uptake analysis was performed on *nu/nu* mice bearing LNCaP tumors and *nu/nu* orchiectomized mice bearing 22Rv1 tumors. For ^{18}F-FDHT PET imaging experiments, 4 *nu/nu* mice bearing LNCaP tumors and 4 orchiectomized *nu/nu* mice bearing 22Rv1 tumors were used. For SHBG-^{18}F-FDHT PET imaging, 4 LNCaP and 8 22RV1 tumor–bearing mice were used, with the 22Rv1 tumor–bearing mice being divided randomly into 2 equal groups receiving either vehicle or enzalutamide (20 mg/kg) 12 h and 1 h before injection. ^{18}F-FDHT and SHBG-^{18}F-FDHT were prepared at 37–179 MBq/mL (3–16 ng of FDHT by mass) in normal saline and injected intravenously. PET/CT images were acquired on a Triumph small-animal PET/CT device (GE Healthcare) for 15 min at a single bed position at 1, 2.5, or 4 h after injection. Images were reconstructed by 3-dimensional ordered-subsets expectation maximization using 4 subsets and 15 iterations. Tumor and heart (as blood pool background) PET signal was quantified by drawing a 3-dimensional region of interest using CT anatomic guidance on VivoQuant software (version 2.5; InviCRO).

Statistical Analysis

Statistical analysis and graphing were performed using Prism software (version 6; GraphPad Software). Differences in cell uptake

were compared using 1-way ANOVA. Differences in ^{18}F-FDHT and SHBG-^{18}F-FDHT competitive inhibition in vitro were analyzed using a Student *t* test. Differences in tumor uptake were compared using 2-way ANOVA.

RESULTS

^{18}F-FDHT Synthesis, Purification, and Analysis

^{18}F-FDHT was synthesized using a modification of a previously described procedure (*13*). Nonradioactive peaks were analyzed by ultraviolet absorbance (210 nM) with an approximately 19-min retention time of ^{18}F-FDHT (retention factor, 7.63) (Fig. 1A). The collected final purified product afforded an injectable solution of ^{18}F-FDHT with an average radiochemical yield of 40% ± 12% (end of synthesis, decay-corrected) and specific activity of 340 ± 55 GBq/μmol (end of synthesis). The purity of the final formulated product was more than 99%, and the retention time matched the FDHT standard (6.1 min). After confirmation of identity and radiochemical purity, we tested ^{18}F-FDHT for specificity and affinity to the AR using cell-binding assays. In highly AR-expressing LNCaP cells, ^{18}F-FDHT uptake was measured at $3.05 \pm 0.49 \times 10^5$ counts per minute (CPM)/mg of protein. The moderately AR-expressing 22Rv1 cell line 22RV1 accumulated significantly lower levels of tracer, at $6.16 \pm 0.21 \times 10^4$ (CPM)/mg of protein, and the AR-negative PC3 cells showed nonspecific background activity of $1.95 \pm 0.50 \times 10^4$ CPM/mg (Fig. 1B). The AR antagonist enzalutamide demonstrated a dose-dependent blockade of binding. Furthermore, enzalutamide was able to decrease ^{18}F-FDHT binding by 82% in LNCaP cells at a concentration of 100 μM, a level comparable to the nonspecific background activity measured in PC3 cells (Fig. 1C). Taken together, these data confirmed that the synthesized compound was biologically active for in vivo analysis.

In Vivo Analysis of ^{18}F-FDHT

To test ^{18}F-FDHT in a variety of biologic settings, 2 models, androgen-sensitive LNCaP tumors and castration-resistant 22Rv1 tumors, were chosen for analysis. The 22Rv1 tumors were investigated in the setting of orchiectomy, since their growth is independent of androgen signaling. Despite the use of 2 models with marked differences in AR expression with and without androgen deprivation, low tracer accumulation was observed across all groups. Specific tumor uptake, as measured by a ratio of mean tumor intensity divided by mean left ventricle intensity (tumor-to-background ratio [TBR]) was below 1 in all groups when measured at 1 h after injection (Fig. 2A). Intact LNCaP mice had an average TBR of 0.84 ± 0.12, and orchiectomized 22Rv1 tumor–bearing mice had an average TBR of 0.81 ± 0.08 (Fig. 2B). Visualization of tracer accumulation was consistent with previous murine examinations of ^{18}F-FDHT, with hepatobiliary, bowel, and bone accumulation evident at 1 h after injection.

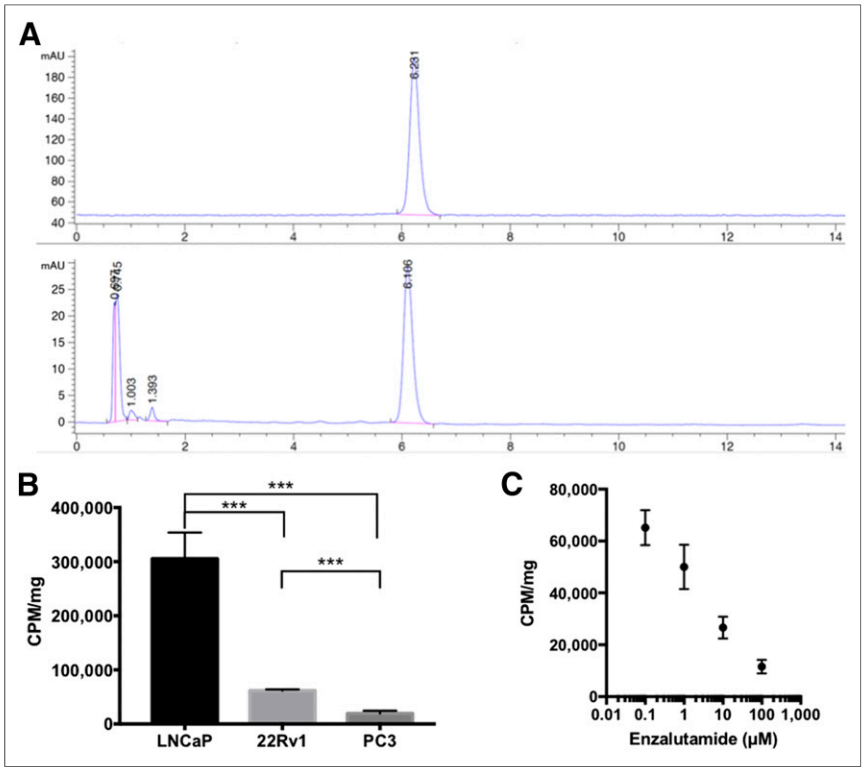

FIGURE 1. (A) High-pressure liquid chromatography radiographic (top) and ultraviolet (bottom) traces after ^{18}F-FDHT synthesis. ^{18}F-FDHT peaks detected by both ultraviolet (210 nM) and radioactive traces were consistent with successful synthesis of target molecule. (B) ^{18}F-FDHT uptake measured in high-AR (LNCaP), moderate-AR (22Rv1), and low-AR (PC3) cells. Bars represent mean of 6 replicates, with error bars denoting SEM. (C) Competitive binding of enzalutamide to LNCaP cells, demonstrating dose-dependent decrease of ^{18}F-FDHT uptake with increasing doses of enzalutamide. Dots represent mean of 6 samples quantified by γ-counter and measured in CPM and normalized to total protein, with error bars denoting SEM. ***$P < 0.001$.

In Vitro Comparison of ^{18}F-FDHT and SHBG-^{18}F-FDHT

SHBG was bound to ^{18}F-FDHT, and the combined molecule was compared with ^{18}F-FDHT alone across several in vitro analyses. The stability and functionality of both ^{18}F-FDHT and SHBG-^{18}F-FDHT under different serum conditions were assessed, measuring cell-bound activity as an output. The binding of ^{18}F-FDHT did not differ from that of SHBG-^{18}F-FDHT in phosphate-buffered saline ($5.12 \pm 2.15 \times 10^5$ vs. $3.40 \pm 0.28 \times 10^5$ CPM/mg, respectively), bovine serum ($4.48 \pm 0.94 \times 10^5$ vs. $3.37 \pm 0.56 \times 10^5$ CPM/mg, respectively), or mouse serum ($3.75 \pm 0.74 \times 10^5$ vs. $3.11 \pm 0.75 \times 10^5$ CPM/mg, respectively) (Fig. 3A). To test the specificity of both tracers, competitive binding experiments with the AR antagonist enzalutamide were used. Specific binding and nonspecific binding were similar for both tracers at 1 h (unblocked: ^{18}F-FDHT = $5.04 \pm 0.50 \times 10^5$ CPM/mg, SHBG-^{18}F-FDHT = $5.50 \pm 0.93 \times 10^5$ CPM/mg; blocked/unspecific: ^{18}F-FDHT = $1.19 \pm 0.52 \times 10^5$ CPM/mg, SHBG-^{18}F-FDHT = $1.27 \pm 0.38 \times 10^5$ CPM/mg), with similar percentages of blocking achieved, at 76% and 77%, for ^{18}F-FDHT and SHBG-^{18}F-FDHT, respectively. Enzalutamide was also assayed for competitive binding with ^{18}F-FDHT for SHBG. Minimal ^{18}F-FDHT displacement occurred across a range of concentrations, and even at concentrations

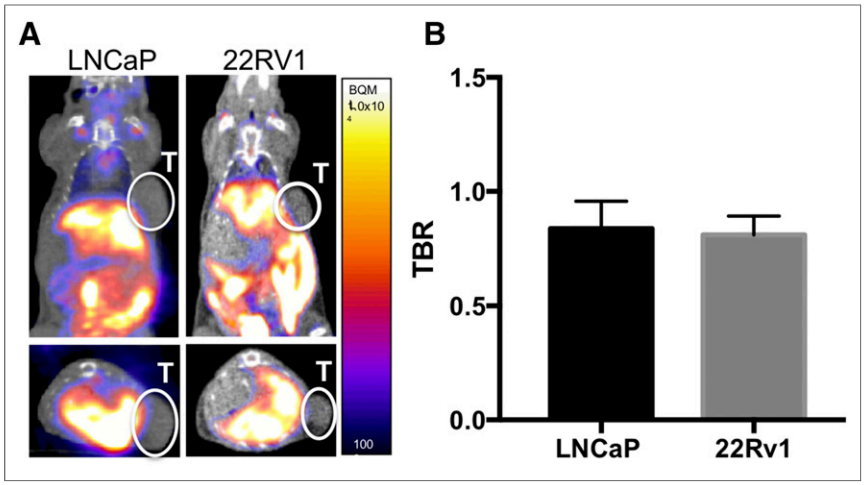

FIGURE 2. (A) Coronal (top) and axial (bottom) images of mice bearing LNCaP and 22Rv1 human prostate cancer xenografts 1 h after injection with ^{18}F-FDHT. Signal accumulation is consistent with previously observed hepatobiliary clearance of tracer, with no accumulation visualized in either tumor. (B) Tumor uptake normalized for injection by comparison to left ventricle uptake in LNCaP and 22Rv1 mice. Bars represent mean of 4 replicates, with error bars representing SEM. T = tumor.

as high as 100 μM, up to 57% of the ^{18}F-FDHT remained bound, indicating that enzalutamide did not affect the SHBG-^{18}F-FDHT complex. Finally, the kinetics of both ^{18}F-FDHT and SHBG-^{18}F-FDHT were assayed over 4 h. Although there was similar uptake at both 1 and 2.5 h for free ^{18}F-FDHT (1 h, 5.50 ± 0.46 × 10^5 CPM/mg; 2.5 h, 2.03 ± 0.19 × 10^5 CPM/mg) and bound ^{18}F-FDHT (1 h, 5.04 ± 0.35 × 10^5 CPM/mg; 2.5 h, 2.40 ± 0.34 × 10^5 CPM/mg), at 4 h a significant increase occurred for the SHBG-bound ^{18}F-FDHT (4.32 ± 0.14 × 10^5 CPM/mg of ^{18}F-FDHT vs. 1.04 ± 0.06 × 10^6 CPM/mg of SHBG-^{18}F-FDHT, $P <$ 0.0001), as shown in Figure 3D. These results provide evidence that SHBG decisively changes the kinetics of specific ^{18}F-FDHT binding.

In Vivo Comparison of ^{18}F-FDHT and SHBG-^{18}F-FDHT

Purified ^{18}F-FDHT was bound to SHBG before injection in a similar manner to in vitro experiments, and uptake was quantified over time in intact LNCaP and orchiectomized 22Rv1 tumor–bearing mice. The 22Rv1 mice were randomly distributed into vehicle and enzalutamide-treated groups to test for specificity. At 1 h after injection, the TBRs of LNCaP (0.72 ± 0.12), 22Rv1 (0.94 ± 0.14), and enzalutamide-blocked 22Rv1 tumors (0.74 ± 0.06) for SHBG-bound ^{18}F-FDHT were all statistically similar. The TBRs for both LNCaP and 22Rv1 tumors were also similar between free and SHBG-bound ^{18}F-FDHT. The similarity between the 2 groups existed despite a significantly lower blood signal in the free ^{18}F-FDHT group (Fig. 4C), indicating that although there are differences in clearance of the 2 tracers at 1 h, the tumor accumulation at 1 h does not appear to be specific for any group. Given the evidence that free ^{18}F-FDHT was significantly more metabolized at 1 h, only SHBG-bound ^{18}F-FDHT was analyzed at later time points (Fig. 4). For SHBG-^{18}F-FDHT, TBRs increased in both blocked and unblocked 22Rv1 tumors from 1 to 2.5 h, with TBR levels increasing to 1.00 ± 0.19 in 22Rv1 and 1.21 ± 0.02 in enzalutamide-blocked 22Rv1 tumors. No increase was observed at 2.5 h in the intact LNCaP prostate cancer model. At 2.5 h after injection, a significant difference in TBR was observed between the 22Rv1 and LNCaP models. At 4 h after injection, a statistically significant divergence in TBR was observed between blocked and unblocked AR in 22Rv1 tumors. Unblocked 22Rv1 tumors demonstrated the highest TBR, at 1.62 ± 0.26, followed by enzalutamide-blocked 22Rv1 tumors, at 1.07 ± 0.13, and finally LNCaP tumors, at 0.56 ± 0.19. These differences were driven by a significant increase in the TBR of 22Rv1 tumors, which was not observed in either the AR-blocked or the intact LNCaP tumor models. This finding confirmed the observed in vitro data, indicating SHBG-mediated AR-specific ^{18}F-FDHT uptake in prostate cancer xenografts at 4 h.

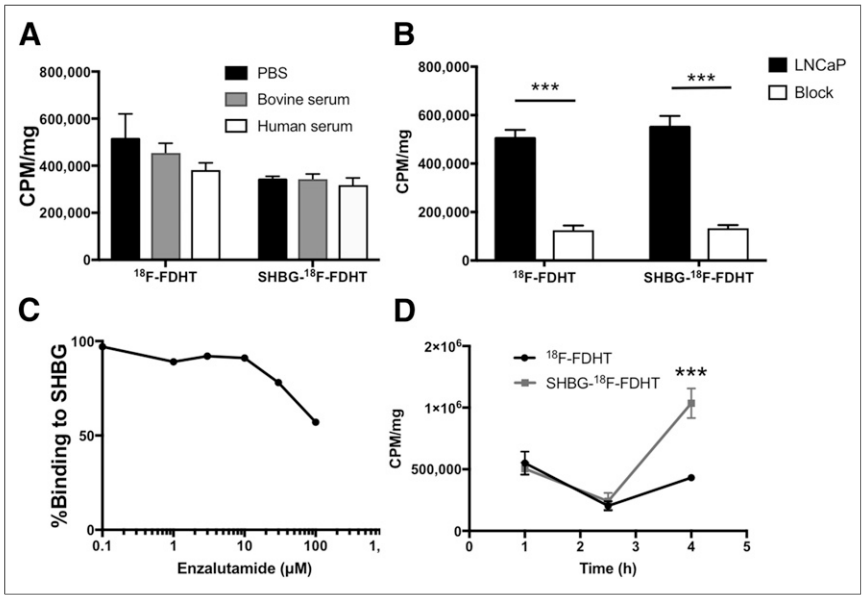

FIGURE 3. (A) Uptake of ^{18}F-FDHT and SHBG-^{18}F-FDHT in LNCaP cells after 1 h of incubation in phosphate-buffered saline (PBS), bovine serum, or human serum, standardized by protein per well. Bars represent mean of 6 replicates, and error is denoted by SEM. (B) Competitive binding analysis of ^{18}F-FDHT and SHBG-^{18}F-FDHT with AR antagonist enzalutamide. Each bar is mean of 6 replicates ± SEM. (C) Competitive binding analysis of ^{18}F-FDHT to SHBG with AR antagonist enzalutamide, demonstrating minimal competition between ^{18}F-FDHT and enzalutamide for binding to SHBG. (D) Time course of ^{18}F-FDHT and SHBG-^{18}F-FDHT binding to LNCaP cells. Although similar levels of binding are observed at 1 and 2.5 h, significant increase in uptake is seen at 4 h in only cells incubated with SHBG-^{18}F-FDHT. Dots represent mean of 6 replicates ± SEM. ***$P <$ 0.001.

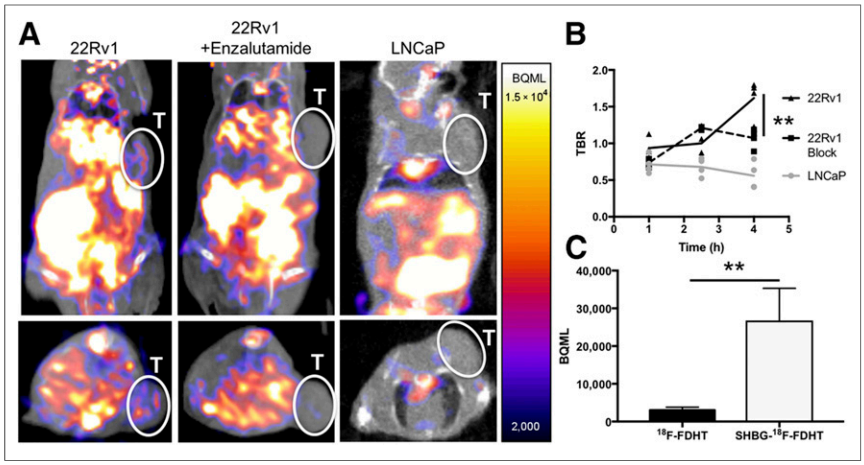

FIGURE 4. (A) Coronal (top) and axial (bottom) images of 22Rv1, 22Rv1-plus-enzalutamide, and LNCaP tumor–bearing mice 4 h after injection with SHBG-^{18}F-FDHT. Hepatobiliary clearance is similar to that of ^{18}F-FDHT; however, accumulation is also visualized in ^{18}F-FDHT-SHBG–injected 22Rv1 mice. (B) Time course quantification of tumor accumulation standardized to injection as TBR. Each dot represents individual mouse from 22Rv1, 22Rv1 block, and LNCaP groups. (C) Blood levels quantified by PET for ^{18}F-FDHT and SHBG-^{18}F-FDHT. $^{**}P < 0.01$. T = tumor.

DISCUSSION

The work herein demonstrates a novel method to quantify AR expression differences in mouse models of prostate cancer with PET imaging by using ^{18}F-FDHT bound to SHBG and imaging at prolonged time points. Our work confirmed that although ^{18}F-FDHT alone is capable of specifically binding the AR in vitro, there is no specific uptake of ^{18}F-FDHT in human prostate cancer xenografts in mice. Previous studies have investigated accumulation in mature and immature rodent prostate and models of human ovarian cancer and glioma, but thus far prostate cancer had not been analyzed (*10,14*). Although each model has demonstrated AR expression, the levels of AR expression in prostate cancer are more clinically relevant, since most AR-targeted therapies aim to manage both castration-sensitive and refractory prostate cancer (*15–17*). Thus, successful ^{18}F-FDHT imaging in a murine model of prostate cancer might not only aid development of these AR-targeted therapies but also contribute to the knowledge of ^{18}F-FDHT accumulation that is mediated by SHBG. We hypothesized that a more systematic examination of the role of SHBG in ^{18}F-FDHT rodent animal models could facilitate successful imaging.

Although SHBG is best known for its ability to modulate the levels of free steroids in the blood, the protein is also capable of binding cells and initiating signaling in cancer cells, including prostate cancer (*18,19*). ^{18}F-FDHT has been studied extensively both in vitro and in vivo, but no data have been reported in vitro when bound to SHBG. Conversely, a large body of work centered around the free-hormone hypothesis has investigated various facets of SHBG and dihydrotestosterone cell binding and their respective internalization and signaling. Our data agree with the work by Hammes et al., demonstrating uptake of both SHBG and dihydrotestosterone by rat choriocarcinoma cells (*20*), which was postulated to occur through megalin-induced endocytosis. Our work expanded on this analysis to include uptake over time and a direct comparison of the uptake of free ^{18}F-FDHT and SHBG-bound ^{18}F-FDHT. Because the dissociation half-life of dihydrotestosterone from SHBG is on the order of 43 s (*21*), early-time-point binding may reflect more heavily on the dissociated ^{18}F-FDHT, which would explain similar uptake at early time points. The use of a competitive antagonist also supports this hypothesis, as most of the cell-associated signal is blocked by the addition of enzalutamide. We hypothesize that differences in accumulation at later time points occur, at least in part, because of the biology of SHBG internalization. Free SHBG has been demonstrated to bind megalin and to be endocytosed, resulting in accumulating cytoplasmic levels of the protein (*22*). Once internalized, SHBG is able to retard the efflux of ^{18}F-FDHT (*20*), providing an additional mechanism of enhanced ^{18}F-FDHT retention and therefore a larger pool of tracer capable of binding the AR. Given the slow association of SHBG to cellular membranes (*23*), it is likely that only at the 4-h time point is accumulation driven by this protective or reservoir effect (*24*).

The observation that SHBG-bound ^{18}F-FDHT potentially had different binding kinetics from free ^{18}F-FDHT in vitro provided a significant impetus to continue the examination in vivo. The similar results observed in vivo also supported the hypothesis that SHBG plays multiple roles in specific ^{18}F-FDHT delivery to the tumor. The significant decrease in measured blood radioactivity for unbound ^{18}F-FDHT in comparison to bound ^{18}F-FDHT signals an increased stability that would be expected of a steroid carrier. Additionally, the dissociation rate of 43 s would provide sufficient time for the SHBG-^{18}F-FDHT complex to be delivered to the tumor. In the tumor microenvironment, the enhanced permeability and retention effect probably also contributes to indistinguishable differences at early time points, which can be clarified over time as SHBG diffuses out of the tumor microenvironment. One limitation of this work is that ^{18}F-FDHT that has dissociated from SHBG after injection cannot be discerned from SHBG-bound tracer, but this limitation does not rule out other potential significant interactions with proteins such as albumin.

In addition to the exploration of SHBG-^{18}F-FDHT kinetics, examination of biologically distinct human tumor xenografts provided additional considerations for successful rodent imaging. The universally low ^{18}F-FDHT accumulation, whether SHBG-bound or free, in LNCaP xenografts emphasizes that the presence of endogenous sex hormones makes a significant difference in murine models. Although the most likely explanation for the significantly lower accumulation is direct competition of endogenous hormones with ^{18}F-FDHT, other, yet-unknown, effects of orchiectomy could contribute to increased accumulation in 22Rv1 tumors.

CONCLUSION

The role of the AR in prostate cancer development, recurrence, and morbidity has been well defined. As such, numerous therapies that target the AR are under development and currently in clinical trials. Although large-scale preclinical ex vivo examinations of the effects of any drug on AR expression or tumor growth can be accomplished ex vivo, the ability to monitor both simultaneously and repeatedly over time to follow the individual response to

therapy cannot be accomplished without molecular imaging. By prebinding ^{18}F-FDHT with SHBG, we showed the possibility of specifically imaging ARs in human prostate cancer xenograft mouse models. This procedure might permit novel therapeutic strategies targeting AR and deepen our understanding of the kinetics of AR receptor signaling.

DISCLOSURE

This work was supported by DOD synergistic award W81XWH-14-1-0406 to Umar Mahmood and Massimo Loda. No other potential conflict of interest relevant to this article was reported.

REFERENCES

1. Joseph DR. Structure, function, and regulation of androgen-binding protein/sex hormone-binding globulin. *Vitam Horm.* 1994;49:197–280.
2. Treatment and survival of patients with cancer of the prostate. The Veterans Administration Co-operative Urological Research Group. *Surg Gynecol Obstet.* 1967;124:1011–1017.
3. Scher HI, Heller G. Clinical states in prostate cancer: toward a dynamic model of disease progression. *Urology.* 2000;55:323–327.
4. Agus DB, Cordon-Cardo C, Fox W, et al. Prostate cancer cell cycle regulators: response to androgen withdrawal and development of androgen independence. *J Natl Cancer Inst.* 1999;91:1869–1876.
5. Isaacs JT, Coffey DS. Adaptation versus selection as the mechanism responsible for the relapse of prostatic cancer to androgen ablation therapy as studied in the Dunning R-3327-H adenocarcinoma. *Cancer Res.* 1981;41:5070–5075.
6. Shah RB, Mehra R, Chinnaiyan AM, et al. Androgen-independent prostate cancer is a heterogeneous group of diseases: lessons from a rapid autopsy program. *Cancer Res.* 2004;64:9209–9216.
7. Eichler K, Hempel S, Wilby J, Myers L, Bachmann LM, Kleijnen J. Diagnostic value of systematic biopsy methods in the investigation of prostate cancer: a systematic review. *J Urol.* 2006;175:1605–1612.
8. Larson SM, Morris M, Gunther I, et al. Tumor localization of 16β-^{18}F-fluoro-5α-dihydrotestosterone versus ^{18}F-FDG in patients with progressive, metastatic prostate cancer. *J Nucl Med.* 2004;45:366–373.
9. Dehdashti F, Picus J, Michalski JM, et al. Positron tomographic assessment of androgen receptors in prostatic carcinoma. *Eur J Nucl Med Mol Imaging.* 2005;32:344–350.
10. Downer JB, Jones LA, Engelbach JA, et al. Comparison of animal models for the evaluation of radiolabeled androgens. *Nucl Med Biol.* 2001;28:613–626.
11. Danzo BJ, Eller BC. Steroid-binding proteins in rabbit plasma: separation of testosterone-binding globulin (TeBG) from corticosteroid-binding globulin (CBG), preliminary characterization of TeBG, and changes in TeBG concentration during sexual maturation. *Mol Cell Endocrinol.* 1975;2:351–368.
12. Karr JP, Kirdani RY, Murphy GP, Sandberg AA. Sex hormone binding globulin and transcortin in human and baboon males. *Arch Androl.* 1978;1:123–129.
13. Zhou D, Lin M, Yasui N, et al. Optimization of the preparation of fluorine-18-labeled steroid receptor ligands 16alpha-[^{18}F]fluoroestradiol (FES), [^{18}F]fluoro furanyl norprogesterone (FFNP), and 16beta-[^{18}F]fluoro-5alpha-dihydrotestosterone (FDHT) as radiopharmaceuticals. *J Labelled Comp Radiopharm.* 2014;57:371–377.
14. Khayum MA, Doorduin J, Antunes IF, et al. In vivo imaging of brain androgen receptors in rats: a [^{18}F]FDHT PET study. *Nucl Med Biol.* 2015;42:561–569.
15. Horoszewicz JS, Leong SS, Kawinski E, et al. LNCaP model of human prostatic carcinoma. *Cancer Res.* 1983;43:1809–1818.
16. Scher HI, Sawyers CL. Biology of progressive, castration-resistant prostate cancer: directed therapies targeting the androgen-receptor signaling axis. *J Clin Oncol.* 2005;23:8253–8261.
17. Montgomery B, Eisenberger MA, Rettig MB, et al. Androgen receptor modulation optimized for response (ARMOR) phase I and II studies: galeterone for the treatment of castration-resistant prostate cancer. *Clin Cancer Res.* 2016;22:1356–1363.
18. Mean F, Pellaton M, Magrini G. Study on the binding of dihydrotestosterone, testosterone and oestradiol with sex hormone binding globulin. *Clin Chim Acta.* 1977;80:171–180.
19. Nakhla AM, Rosner W. Stimulation of prostate cancer growth by androgens and estrogens through the intermediacy of sex hormone-binding globulin. *Endocrinology.* 1996;137:4126–4129.
20. Hammes A, Andreassen TK, Spoelgen R, et al. Role of endocytosis in cellular uptake of sex steroids. *Cell.* 2005;122:751–762.
21. Mendel CM. Rates of dissociation of sex steroid hormones from human sex hormone-binding globulin: a reassessment. *J Steroid Biochem Mol Biol.* 1990;37:251–255.
22. Hryb DJ, Khan MS, Romas NA, Rosner W. The control of the interaction of sex hormone-binding globulin with its receptor by steroid hormones. *J Biol Chem.* 1990;265:6048–6054.
23. Hryb DJ, Khan MS, Romas NA, Rosner W. Solubilization and partial characterization of the sex hormone-binding globulin receptor from human prostate. *J Biol Chem.* 1989;264:5378–5383.
24. Hong E-J, Sahu B, Jänne OA, Hammond GL. Cytoplasmic accumulation of incompletely glycosylated SHBG enhances androgen action in proximal tubule epithelial cells. *Mol Endocrinol.* 2011;25:269–281.